RSC Advances

PAPER

View Article Online
View Journal | View Issue

Cite this: *RSC Adv.*, 2024, **14**, 16421

Highly efficient aramid fiber supported polypropylene membranes modified with reduced graphene oxide based metallic nanocomposites: antimicrobial and antiviral capabilities

Kiran Mustafa,[ab] Nadeem Iqbal,[c] Sajjad Ahmad,[d] Sadia Iqbal,[a] Mashallah Rezakazemi,[e] Francis Verpoort,[fg] Javaria Kanwal[a] and Sara Musaddiq *[a]

Received 29th January 2024
Accepted 8th April 2024

DOI: 10.1039/d4ra00724g

rsc.li/rsc-advances

Polypropylene hybrid polymeric membranes with aramid support have been fabricated using Thermally Induced Phase Separation (TIPS). Different modifying materials, such as metallic nanoparticles and reduced graphene oxide (rGO), improve the properties of these membranes. The nanomaterials and the fabricated membranes have been characterized with FTIR spectrometer, SEM and UV-Vis Spectrophotometer. Following that, the disinfection capabilities of the fabricated hybrid membranes were investigated. The antibacterial capability of the membranes is established through the testing of the membranes against bacterial strains *S. aureus* and *E. coli*, whereas the antiviral evaluation of the membranes was made against *H9N2* and *IBV* strains. This research aims to develop advanced hybrid membranes that effectively disinfect water by incorporating novel nanomaterials and optimizing fabrication techniques.

1. Introduction

In water purification, addressing the persistent issue of removing sophisticated contaminants — encompassing pharmaceuticals, pesticide residues, dyes, and diverse industrial by-products — extends beyond the scope of traditional methods such as biochemical degradation and sedimentation. The conventional water treatment process is a multi-tiered system starting with primary treatment for suspending particulates through macro-filtration, followed by secondary treatment deploying oxidation to eliminate biological matter. Subsequent tertiary treatments include disinfection using various chemicals like chlorine, chlorine dioxide, and ozone, with ultraviolet (UV) radiation intermittently applied as a disinfectant. Once treated, this water re-enters the ecosystem, particularly in agricultural sectors.[1]

The industrialized practice of water purification has increasingly integrated membrane technology post-primary treatment, vastly expanding the array of filterable contaminants and presenting a purification method that balances energy efficiency with cost-effectiveness. The functionality of polymeric membranes is distinguished, although the issue of biofouling presents significant operational challenges, curtailing membrane life, necessitating recurring flux maintenance, and precipitating a marked flux decline that calls for complex, multistage purification strategies.[2] Engineering membranes with anti-biofouling features is vital to leverage their full potential. Recent advancements in polymeric membrane technology have yielded membranes capable of innately resisting microbial threats.[3]

These optimized antimicrobial polymeric membranes are constructed as thin polymeric films of varying thickness, chemically treated with agents such as nanoparticles, imparting advantageous properties to the membranes. Diverse filtration techniques such as microfiltration (MF), nanofiltration (NF), ultrafiltration (UF), and reverse osmosis (RO) represent the spectrum of membrane-based water purification, with MF and UF often serving as precursors to NF and RO processes. RO membranes, particularly utilized in desalination to treat water with high "Total Dissolved Solids (TDS)", are limited to removing dissolved inorganic substances and are vulnerable to

[a]*Department of Chemistry, The Women University, Multan 66000, Pakistan. E-mail: drsara.chem@wum.edu.pk*
[b]*Govt. Graduate College (W), Higher Education Department, Khanewal, Punjab, Pakistan*
[c]*Director Microtech Chemicals and Minerals, Kasur 55050, Punjab, Pakistan*
[d]*Pakistan Council of Research in Water Resources, Ministry of Water Resources, Islamabad, Pakistan*
[e]*Faculty of Chemical and Materials Engineering, Shahrood University of Technology, Shahrood 9WVR+757, Iran*
[f]*State Key Laboratory of Advanced Technology for Materials Synthesis and Processing, Wuhan University of Technology, Wuhan 430070, China*
[g]*National Research Tomsk Polytechnic University, Lenin Avenue 30, 634050 Tomsk, the Russian Federation*

damage upon contact with organic liquids. This limitation and their high maintenance and energy demands underscores the necessity for more cost-efficient and efficient technologies.[4]

Amid economic and societal considerations, alongside membrane techniques' efficacy, there's a pressing need to innovate less costly, more efficient wastewater purification technologies. Commonly used polymers for creating water purification membranes include cellulose acetate (CA), polyvinylidene fluoride (PVDF), polyamide (PA), and polysulfone. These hybrid polymeric membranes can acquire novel attributes by incorporating a variety of additives into the membrane casting solutions, tailored according to the desired membrane functionality, spanning inorganic to organic compounds.[5]

Polymeric membranes with inherent antibacterial properties are rare. A support or pure polymer membrane does not confer antibacterial features; these are imparted by adding specific modifying compounds to the membrane's polymer matrix, bolstering the membrane's bactericidal capabilities. Some modifications enhance surface properties for better rejection rates or improved flux recovery, while others demonstrate efficacy against various bacterial strains. Organic compounds, such as thiazoles, oxazoles, and their derivatives, are notable for their exceptional antibacterial properties.[6] Addressing biofouling — the inevitable microbial adhesion and colonization on membrane surfaces in filtration systems — antimicrobial membranes emerge as a potent defense. These membranes not only reduce biofouling but also contribute to eradicating free-floating microbes or spores, and despite viruses being smaller than the pores, antimicrobials can eliminate them from the stream.[7,8]

Recent studies have demonstrated the antibacterial efficacy of polymeric membranes. For instance, polyether sulfone membranes produced through phase inversion, when enhanced with SiO_2 nanoparticles, displayed an increased flow rate of 150 $Lm^2\ h^{-1}\ bar^{-1}$, with the characterization of the membrane surface and distinctive features elucidated *via* techniques such as Thermal Gravimetric Analysis (TGA), Scanning Electron Microscope (SEM), Fourier Transform Infrared (FTIR) Spectroscopy, and Transmission Electron Microscopy (TEM).[9] Furthermore, composite polypropylene membranes with aramid support have been documented for achieving salt rejection rates of between 70% and 75%.[10]

A groundbreaking approach involves the green synthesis of silver nanoparticles (AgNPs) using Callistemon viminalis flower extracts, applied onto polycarbonate membranes through ultrasonication and centrifugation, inhibiting the growth of both Gram-positive and Gram-negative bacteria effectively, as indicated by surface plasmon resonance at 310 nm.[11]

Fig. 1 shows a log reduction in bacterial colonies caused by distinct modifiers in a particular membrane system.

During water filtering, the antimicrobial membranes are discovered to be effectual against a broad range of microbial strains. *E. coli* causes millions of fatalities annually and is dangerous to humans. Various waterborne diseases are caused by diverse *E. coli* strains, including Shiga toxin-producing enteropathogenic *E. coli*. Like this, enteric diseases such hemolytic uraemic syndrome and others are brought on by enterohaemorrhagic *E. coli*. *E. coli* is resistant to a variety of antibiotics that are utilized by its host because of its frequent exposure to them. *E. coli* is a naturally occurring organism found in the GI tracts of mammals and is dispersed into the environment by fecal deposition. According to certain research, the bacteria can reproduce and live for extended periods outside the digestive system. According to some 1980s studies, gastrointestinal (GI) disorders were directly linked to increased *E. coli* contamination in water from many sources, including sewage, manure, and slaughterhouse wastes. As a result, it is frequently used as a biological indication of water contamination by feces.[12] Getting rid of *E. coli* during the wastewater treatment process is essential. Several hybrid polymeric disinfecting

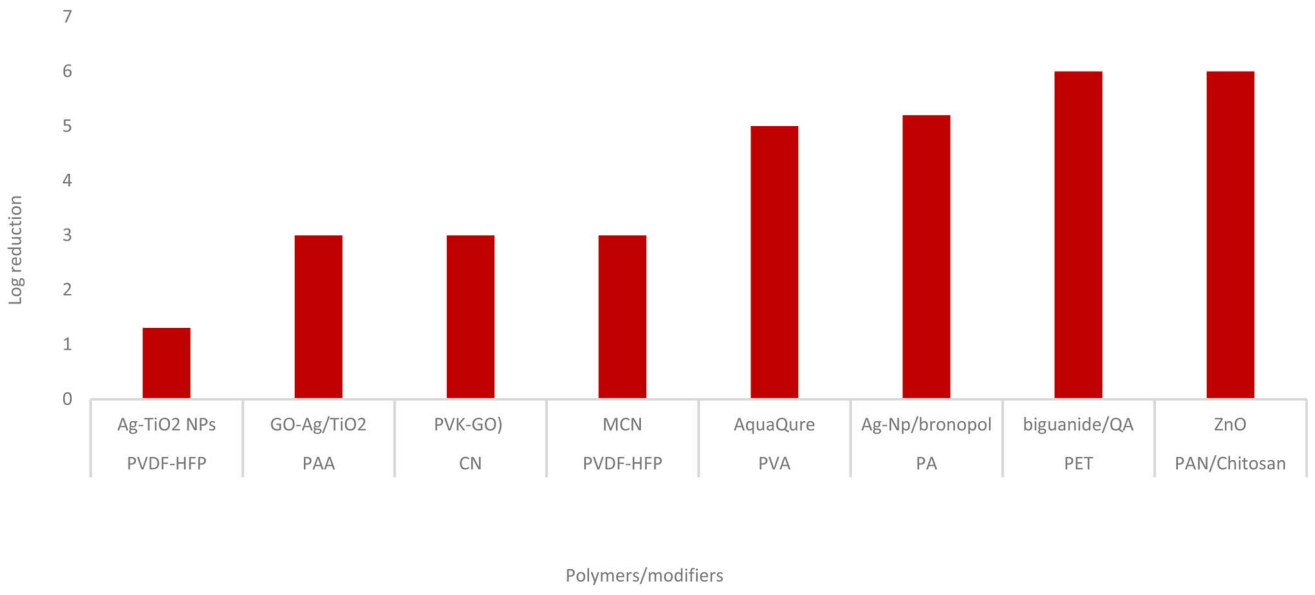

Fig. 1 Different polymeric hybrid membranes' exhibits of bacterial log reduction.

membranes have been created and used to suppress this microorganism during wastewater treatment.

S. aureus is a significant pathogen that still poses a serious threat to world health, mostly because MRSA strains predominate and can cause the deaths of up to 19 000 persons annually in the USA. Wide variety of cytotoxins are produced during the pathogenesis of microbes. The first line of defense against microbial attacks is the inborn immune cells, which the invader can target and kill. Human neutrophils, dendritic cells, and macrophages can all be directly killed by a toxin identified in *S. aureus* leukocidin A/B. Due to its complex reproduction cycle, *S. aureus* uses intricate examining systems to detect a wide range of signals, enabling it to adapt to various environments and modulate its virulence. Human diseases such as superficial skin infections, soft tissue abscesses, endocarditis, pneumonia, toxic shock syndrome, sepsis and are caused by microbes. The microorganism can infect other animals and cause diseases like bovine and ovine mastitis.[13] It is crucial to eliminate the microorganisms from drinking water supplies because of their harmful nature. Several hybrid polymeric membranes are efficient against *S. aureus*.

In a study, an antimicrobial and antifouling PES membrane was developed by incorporating zinc oxide/polyhexamethylene biguanide hydrochloride (ZnO/PHMB) nanocomposites on a commercial PES membrane surface using PDA as an intermediate layer. The fabricated membrane exhibited impressive antimicrobial performance (92.80%), water flux (249.02 LMH), and RB rejection (93.96%), with 91.05% higher water flux after prolonged treatment of secondary effluent.[14]

A study investigated the influence of lateral size and content of graphene oxide (GO) flakes on the anti-biofouling properties and performance of thin-film composite membranes (TFC). Three multidimensional GO samples with varying sizes and degrees of oxidation were prepared and incorporated into the polyamide layer of the TFC membrane. GO1 exhibited excellent bactericidal properties and enhanced desalination performance, while GO2 and GO3 showed significant anti-biofouling effects but negatively impacted water flow due to large-sized sheets and high content of OH-functional groups.[15]

Synthesis of GO modified membranes, phase inversion has found use. For instance, this method recovered 95.3% of the flow by carboxylated-GO/PPYSU augmented membranes. The antibacterial properties of carboxylated-GO make these membranes particularly effective against various microorganisms.[16] Depending on the type of polymer used, phase-inverted GO modified polymeric membranes have different flux rates and rejection percentages. The flow and rejection percentages for specific polymeric membranes are shown in Fig. 2.

In this study, PPY membranes supported by aramid fiber were fabricated. These membranes have been modified with different metallic/rGO nanocomposites. These membranes have been evaluated for the antimicrobial and antiviral activities.

2. Materials and methods

Merck supplied the polypropylene (PPY), isotactic, average Mw 12 000. China's Qingdao Chemical Reagent Co. Ltd. provided

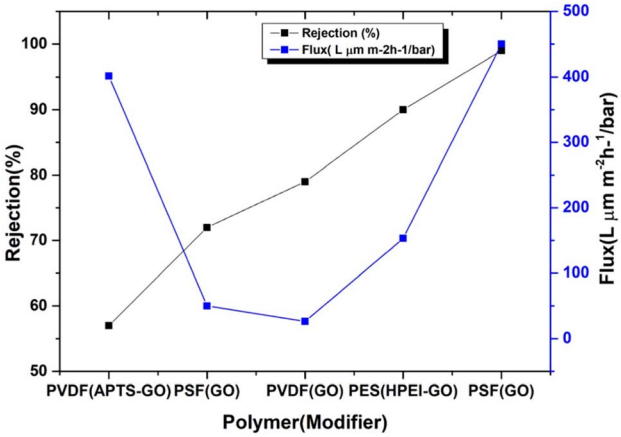

Fig. 2 Rejection percentage and flux rates for various polymeric membranes. Phase inversion is used to create polymeric membranes with GO modifications.

sulphuric acid (98 wt%), cobaltous nitrate hexahydrate, zinc nitrate hexahydrate, tetraammineplatinum(II) nitrate, and graphite flakes $NaNO_3$ (99.0% purity). $CuCl_2$ with a 99.0% purity, ferric nitrate nonahydrate with a 99.0% purity (adipic acid) with a 99.5% purity, cupric nitrate trihydrate with a 98.0% purity, Alsever solution with a 99.0% purity, and sodium polyacrylate was used to purchase Sigma Aldrich 99.0% purity, monobasic potassium phosphate and dibasic sodium phosphate; 99.0% purity. We bought soy oil from a nearby market. Sigma Aldrich purchased *n*-hexane. The reagent grade was used for all the solvents. Sarco Chemical Industries provided 6% hydrogen peroxide. All the experiments used either distilled water or, in some cases, deionized (DI) water.

3. Synthesis of modifiers

3.1. Preparation of nanoparticles (Nps)

3.1.1. ZnO Nps. ZnO Nps were prepared in accordance with a reported process. For this purpose, 0.1 M solution of zinc nitrate hexahydrate and leaf extract of *M. oleifera* were combined, and the fusion was heated for 5 min at a constant temperature while stirring. The solution was then given 1 M NaOH and agitated with constant heating (a hazy solution was formed). Nps were subsequently obtained and separated using centrifugation followed by washing. The Nps was ultimately heated at 60 °C to dry it out.[17]

3.1.2. Fe_2O_3 Nps. Fe_2O_3 Nps were made according to the process outlined by Bhuiyan *et al.*,.[18] For this, *M. oleifera* leaf extract and ferric nitrate nonahydrate 0.2 M solution were combined and the fusion was left to stir until it turned black continuously. The dark solution was then given 1 M NaOH, which was agitated. The solution's pH was kept constant. Thus, produced Nps were centrifuged to separate them before being washed in water. The Nps that had been water-cleaned were eventually heated.

3.1.3. Co_3O_4 Nps. Co_3O_4 Nps were created in accordance with the process outlined by Yulizar *et al.*,.[19] *M. oleifera* leaf extract was added after cobalt nitrate hexahydrate 0.1 M

solution had been heated by stirring at a constant temperature. The solution's hue immediately changed to dark brown as a result. The residue was left in place for the entire night. Thus, the produced Nps were centrifuged to separate them before being washed in water. The Nps that had been water cleaned was eventually heated.

3.1.4. CuO Nps. CuO Nps were created according to the process outlined by Preethi *et al.*[20] *M. oleifera* leaf extract was added to 0.1 M solution of cupric nitrate trihydrate and had been heated. The solution's hue immediately changed from blue to light brown. The answer was left in place for the entire night. Thus, produced Nps were centrifuged to separate them before being washed in water. The object that had been water-cleaned was finally heated.

3.2. Preparation of graphene oxide (GO)

To prepare GO, the improved Hummers approach[21] was applied. To achieve this, sulfuric acid, graphite flakes and sodium nitrate were added. The mixture was then agitated in ice-cold water for 5 to 10 min. The mixture was then gradually added $KMnO_4$ and stirred for 5 days. After 2 h of continuous stirring, an aqueous H_2O_2 solution was added to the mixture. The resulting product was washed twice, once with 0.5% H_2O_2 solution and once with 3% sulphuric acid. The product was then centrifuged after being washed with distilled water. After many washes, the combination yielded the brown/black dispersion of GO.

3.2.1. Plant extract preparation. The *Moringa oleifera* leaves were collected in Multan, Pakistan. *Moringa oleifera* leaves were washed, air-dried at 50 °C for 48 h to ensure thorough dehydration, and ground into a fine powder. The extraction was performed by macerating the powdered leaves in ethanol (70%) for 72 hours at room temperature, ensuring an optimal balance between solvent penetration and compound stability. This methodical approach to drying and extraction times was chosen to maximize the yield and bioactivity of the extract based on empirical evidence suggesting these conditions preserve the integrity and efficacy of the extracted compounds. Literature reports indicate that *Moringa oleifera* extract is rich in bioactive compounds, including flavonoids, phenolic acids, saponins, and alkaloids. These compounds have been quantitatively analyzed to determine their specific concentrations, highlighting the extract's comprehensive phytochemical makeup. Such findings underscore the potential of *Moringa oleifera* extract in water purification applications, leveraging the synergistic effects of its bioactive constituents for enhanced efficacy.[22]

3.3. Preparation of reduced graphene oxide

M. oleifera extract and GO mixture were stirred for 24 h and heated to develop rGO. After the reaction, the resulting liquid was centrifuged and repeatedly rinsed with distilled water to remove all the plant extract-suspended particles. The resulting black product was then dried in an oven.

3.4. Fabrication of membranes

3.4.1. PPYY/rGO membrane: PPY/aramid fiber membrane enhanced with rGO. PPY polymer with oil was heated to 300 °C in a steel container with constant stirring at 450 rpm to create the hot boiling solution at 300 °C to create the PPY/metallic-oxide Nps membranes. All the prepared NPs were collected and sonicated with sodium polyacrylate (dispersant) for 1 h at 25 °C in a separate vial. The heated oil solution is added in this sonicated dispersion and agitated one more to create a homogeneous combination. A piece of Aramid (Kevlar) cloth measuring 4 × 4 cm was submerged in this solution, removed immediately, and then submerged in distilled water. This fabric acted as the support for the membrane. The membrane spent some time in distilled water before spending 12 h in *n*-hexane.

As a result, the oil on the membrane could be removed, and the membrane could then dry. The desalination, degradation, or disinfection capabilities of the produced membrane were then assessed. The PPYY/Fe_2O_3, PPYY/ZnO, PPYY/CO_3O_4 and PPYY/CuO membranes were the names given to the modified PPY membranes with ZnO, Fe_2O_3, Co_3O_4, and CuO respectively. The prepared membranes had a thickness of 10.001 μm. Fig. 3 depicts the diagram for producing and constructing PPY/metallic-oxide Nps membranes.

3.4.2. PPYY/rGO membrane: PPY/aramid fiber membrane modified with rGO. PPY polymer with oil was added to a steel container and heated at 300 °C with constant stirring at 450 rpm to create PPY/rGO membranes. The hot boiling solution was then created, and the temperature was kept at 300 °C. A different vial of 0.05 g of rGO was collected and sonicated for an hour at room temperature with a dispersant (sodium polyacrylate). The heated oil solution received this sonicated dispersion, which was then combined and agitated more to create a homogeneous combination. A piece of Aramid (Kevlar) cloth measuring 4 × 4 cm was submerged in this solution, removed immediately, and then submerged in distilled water. This fabric supports the membrane. The membrane spent some time in distilled water before spending 12 h in *n*-hexane. As a result, the oil on the membrane could be removed, and the membrane could then dry. The desalination, degradation, or disinfection capabilities of the produced membrane were then assessed. Fig. 4 depicts the diagram for producing and constructing rGO/PPY membranes.

3.4.3. Characterization of nanomaterials and membranes. The FTIR study of several nanomaterials and membranes created in this work. The BRUKER ALPHA-E FTIR-1005151 spectrophotometer was used to conduct the analysis. SEM (JEOL 5410) was used to investigate the surface morphology of several membranes before and after chemical modification.

3.4.4. Evaluation of antimicrobial and antiviral ability of membranes. All the fabricated membranes were assessed for antimicrobial and antiviral activities.

3.4.5. Antibacterial evaluation. The bacterial specimen was acquired from the BVH's bacteriology section and cultivated in the biochemistry lab of the University College of Veterinary and Animal Sciences. *E. coli* and *S. aureus* were two amid them. Bacterial media were maintained on nutritive media, and glycerol stocks were produced.

3.4.5.1. Sterilization of media and equipment. Kirby–Bauer and later James employed the agar disc diffusion method to test the antibacterial activity. After being incubated overnight on

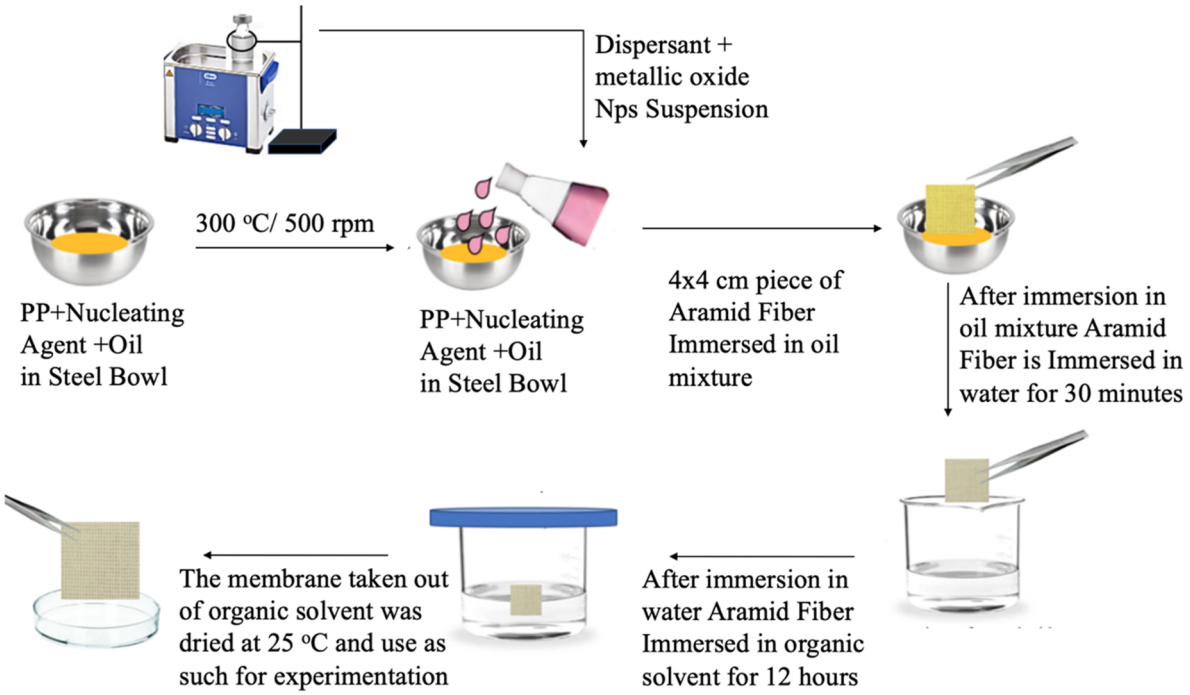

Fig. 3 Nps/PPY membrane fabrication.

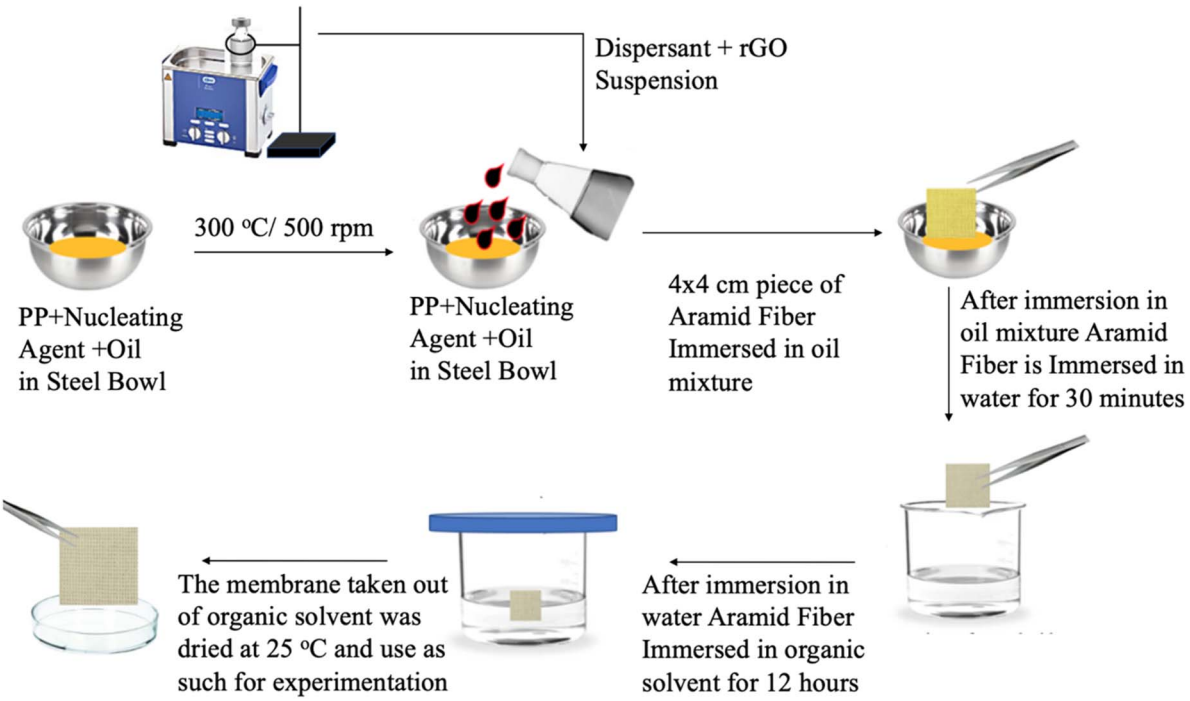

Fig. 4 rGO/PPY membrane fabrication.

agar, a filter paper disc that had been washed with a testing agent had a zone of inhibition.[23] A medium or material is sterilized when all life forms are eliminated. Sterilization is achieved through three methods: dry heat, filtration, and autoclaving. Autoclaving was the most efficient method for sanitizing glassware, tools, and media used for bacterial growth. This study exposed the items to steam at a constant temperature to achieve autoclaving sterilization. Furthermore, to lessen the contamination risk, all the apparatus was dried in an incubator and subsequently autoclaved.

3.4.5.2. Preparation of culture media. Nutrients and a favorable environment are essential for the survival and development of microorganisms. As a result, nutrient mixtures used in the lab to cultivate microorganisms are known as media. As culture media, solid or agar media and liquid or broth media were used. Media preparation was simple because dehydrated products readily accessible on the market were used. Media powder was weighed mixed with distilled water and heated, which were the steps used to prepare the media. After that, an autoclave was used to sterilize it.

3.4.5.3. Transfer, spread, and microbial culture cultivation. Culture dilutions were transferred using micropipettes. A sterile inoculation loop was used to transfer bacteria from one media type to another. The entire experiment, the culture was dispersed around the surface of the agar plate using a sterile glass spreader. Bacteria were cultivated at 37 °C in a shaker-equipped incubator to achieve normal growth.

3.4.5.4. Preparation of agar plates. The aluminum coating on the flask holding the nutritious agar medium was removed. Flames briefly enveloped the neck. The agar medium was instantly poured over the disinfected Petri dishes with the lid held above the dish to avoid contamination. Before the cover was put back on, the agar was given time to cool and firm up. The Petri plates were tilted to prevent moisture from building up on the agar surface.

3.4.5.5. The bacterial culture was reconstituted using stock. The bacteria were streaked from glycerol stocks onto an agar plate to refresh the culture. A liquid sterile broth containing isolated colonies was agitated overnight at constant temperature. After 24 h, the flask was taken from the shaker and many culture aliquots were fabricated.

3.4.5.6. Assay of disc diffusion. In this technique, a plate of agar with a particular bacterial strain against which antibacterial activity is being tested is placed on top of a filter paper or membrane disc carrying a medication or antibacterial component. A clear zone of no development (also called the zone of inhibition) is measured after it has been incubated for the night, all the way around the disc. The medication is either more effective or harmful to the bacterium, depending on the size of the zone.

The disc diffusion procedure was utilized to measure the disinfection capability of the membranes. Evaluating the antibacterial efficacy of several materials at once is easy and useful. Bacteria were raised by introducing the stock strain onto the nutrient broth media. The culture was dispensed in sterile Eppendorf tubes after being refreshed to create various aliquots.

3.4.6. Antiviral evaluation. The sterilized eggs were purchased from a govt. chicken farm Bahawalpur. The viruses were injected into chorioallantoic fluid from embryonic eggs. Prior to virus inoculation, the viability of the embryos was evaluated using the candled method. To clean the eggs, 70% alcohol swabs were used, and then the eggs were placed in new trays. The alcohol was allowed to evaporate before continuing. A category II biosafety cabinet was employed all during the procedure. The bigger ends of the eggs were manually punctured with a sterilized pin, and the virus specimen was swiftly inoculated through the chorioallantoic channel. Eggs were placed in an incubator set at 37 °C, with molten wax used to seal them. The fluids were taken out after 48 to 72 h and put through additional testing, like a hemagglutination test or a haemagglutinin (HA) test, to figure out the virus titer. Before antiviral testing with specific membrane portions, the virus titer was raised after several passes.

3.4.6.1. Cultivation of avian influenza virus H9 strain. In 7–11 day chicken embryonated eggs, the chorioallantoic route was used to generate H9N2. The H9 vaccine was purchased from a nearby Lahore market for this study. The vaccine components were spun to generate clear supernatant. The alum pellet was released. Eggs were allowed to incubat at 37 °C in a moist incubator with daily lighting using the supernatant as an inoculant. The eggs were taken out in a sterile environment. Allantoic fluids were collected 48 h after implantation and stored for future use in sterile Falcon tubes at 4 °C. The H9 virus titer was determined using the HA test in round bottom titer plates. When the HA titer reached 1024, antiviral assays were run, and viral propagation was carried out across several passages.

3.4.6.2. Cultivation of IBV. The IBV was grown in chicken embryonated eggs 7 to 11 days old through the chorioallantoic route. The IBV immunization was employed in this experiment and was procured in Lahore. The fluids were taken out after 48 to 72 h and put through additional testing, like a hemagglutination test or a haemagglutinin (HA) test, to determine the virus titer. When the HA titer reached 2048, antiviral assays were run, and viral propagation was carried out over several passes.

3.4.6.3. Red blood cells RBCs and phosphate buffer saline (PBS) synthesis. The ingredients should be combined in a mixing bowl before making the phosphate buffer saline solution. Distilled water dissolved NaCl, KCl, KH_2PO_4, and $NaHPO_4$. The pH was kept at 7.4. fresh chicken blood was drawn and put in an EDTA-filled falcon tube. Chicken blood was placed in a tube, doubled in volume with PBS, and centrifuged for three minutes at 4000 rpm to produce RBCs. The supernatant was discarded after two to three PBS rinses. By combining recovered RBCs with PBS solution and 1% RBC solution was created. The mixture was then gently incorporated.

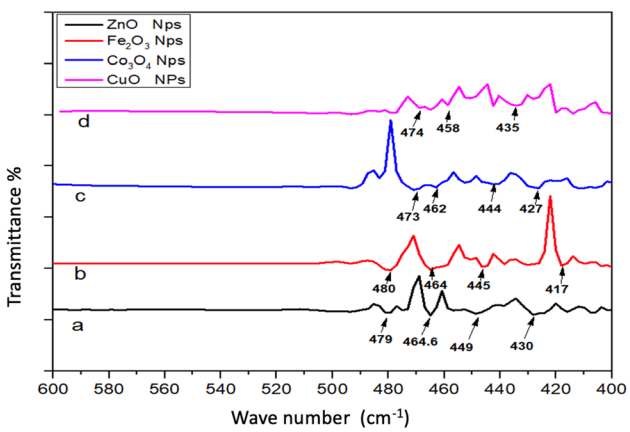

Fig. 5 FTIR spectrum of a = zinc oxide Nps, b = iron oxide Nps, c = Co_3O_4 Nps, d = CuO Nps.

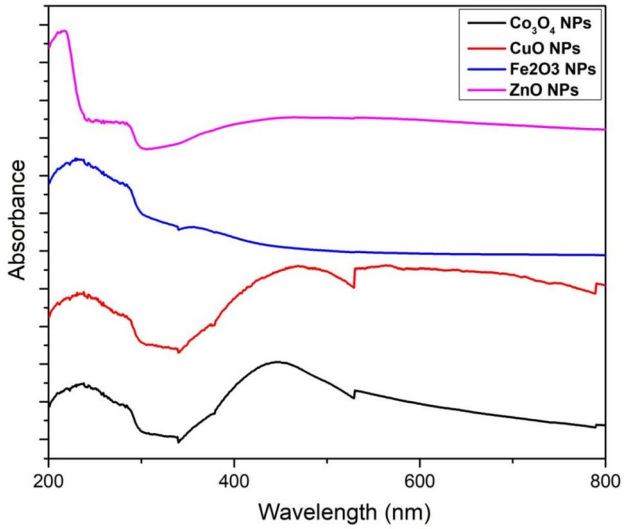

Fig. 6 UV-Visible spectrum of ZnO Nps, Fe_2O_3 Nps, Co_3O_4 Nps, CuO Nps.

3.4.6.4. HA test. Alsever solution and fresh chicken blood were combined in a test tube. After centrifuging RBC-containing blood, the supernatant was collected. This procedure was followed three times. The next step was to combine PBS (pH 7.4) solution with packed RBCs to create a 1% RBC solution. This mixture was added to 50 μl of PBS before being placed into each of the 96 wells of a 96-well plate with a flat bottom. Virus was added to the first well and mixed and was then added to the next well to its right to achieve serial dilution, mixed once more, and continued until the eleventh well. A negative control was used for the 12th well (PBS). 1% RBC solution was gently blended into each well. The plate was incubated at 37 °C to see the results.

3.4.6.5. In ovo antiviral assay. The *in ovo* antiviral assay assessed the membranes' antiviral activity. The membrane fragments were injected into chicken embryonated eggs 7 to 11 days old using the procedure outlined by Rajbhandari *et al.*,.[24] After 48–72 h, all inoculated eggs were collected and analyzed for HA (against IBV and H9 viruses).

4. Results and discussions

4.1. Modifier characterization

All created nanomaterials including nanoparticles and rGO, underwent FTIR and UV analyses. SEM was used to characterize the membranes.

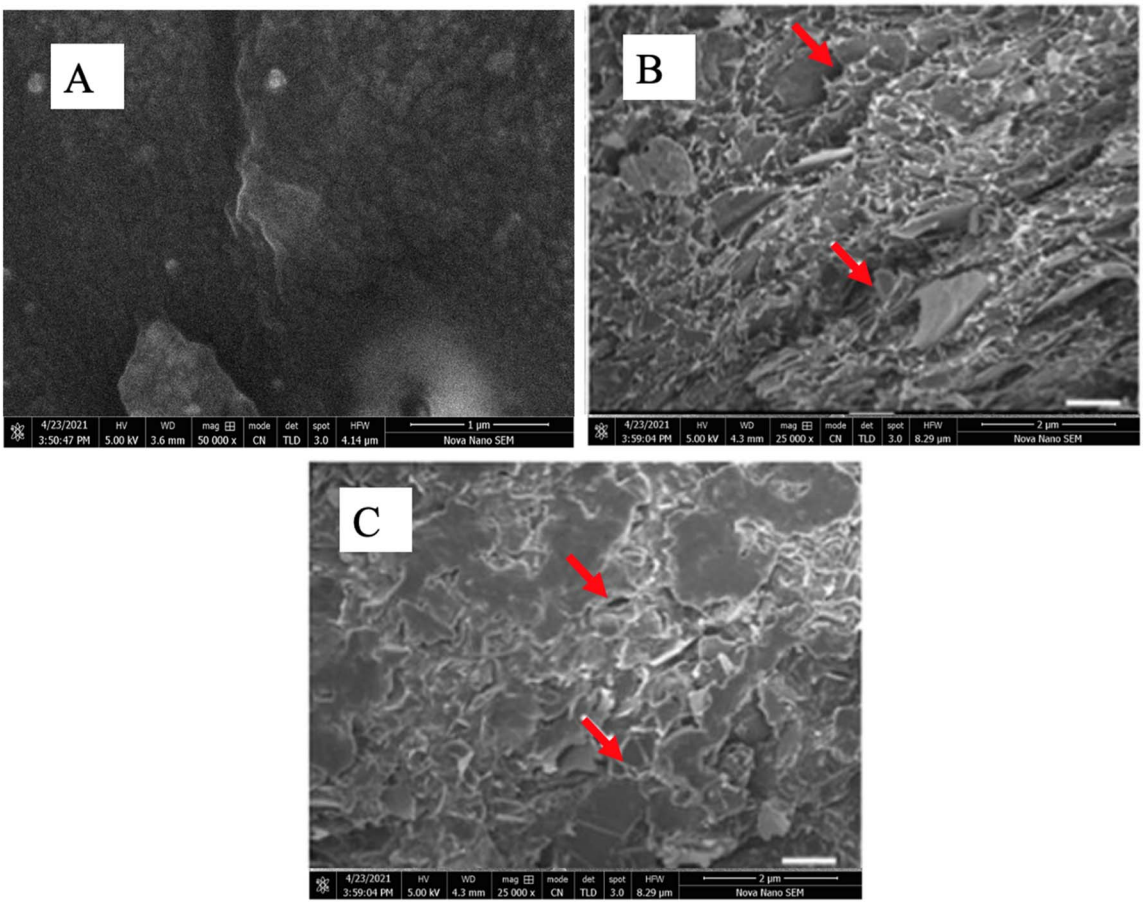

Fig. 7 A = Blank PPYy membrane at 500 00× magnification, B = surface morphological analysis of PPY/ZnO Nps at 250 00× magnification and C = surface morphological analysis of PPY/Fe_2O_3 Nps at 250 00× magnification.

4.2. Fabricated nanoparticles characterization

The stretching vibration of ZnO was visible at 449 cm^{-1} in FTIR spectrum. The emergence of this peak validated the literature's assertion that ZnO Nps had been synthesized.[25] The FTIR spectrum of these Nps is exhibited in Fig. 5. At 472 cm^{-1}, the peak of the Fe–O stretching vibrations was seen. The presence of this peak confirmed the literature's assertion that Fe_2O_3 Nps.[26] The peaks of Co–O stretching vibrations were observed at 473 cm^{-1}. The presence of this band established the fabrication of Co_3O_4 Nps, as reported previously.[27] Cu–O stretching vibrations were observed at 437 cm^{-1}. As reported previously, the band presence established the fabrication of CuO Nps.[28]

Fig. 6 depicts the UV-Vis spectrum of ZnO Nps. The Zn–O adsorption band was seen at 375 nm. The presence of this band corroborated the literature-supported synthesis of Zn–O Nps.[29] At 404 nm, a specific adsorption band of Fe_2O_3 was observed. The presence of this is supported by literature (18). The specific adsorption band of Co_3O_4 was observed at 471 and 275 nm. The adsorption peak of Co_3O_4 Nps emerged within 200–400 nm. The literature validates the peak visible in the spectra.[30] At 475 nm, the CuO adsorption band appeared. According to the literature, the CuO Nps adsorption band emerged between 450 and 500 nm. The literature validates the peaks visible in the spectrum.[31]

4.3. PPY/metallic-oxide Nps membranes characterization

SEM was used to examine PPYy/metallic-oxide Nps membranes series morphologies. Fig. 7 depicts SEM images of all NPs integrated membranes. These membranes were photographed at a magnification of 25 000 at an accelerating voltage of 5.0 kV for electrons with HFWs of 41.4 μm and 8.29 μm at various magnifications. Fig. 7A depicts the smooth surface of the polymer over the aramid fiber. In comparison to the

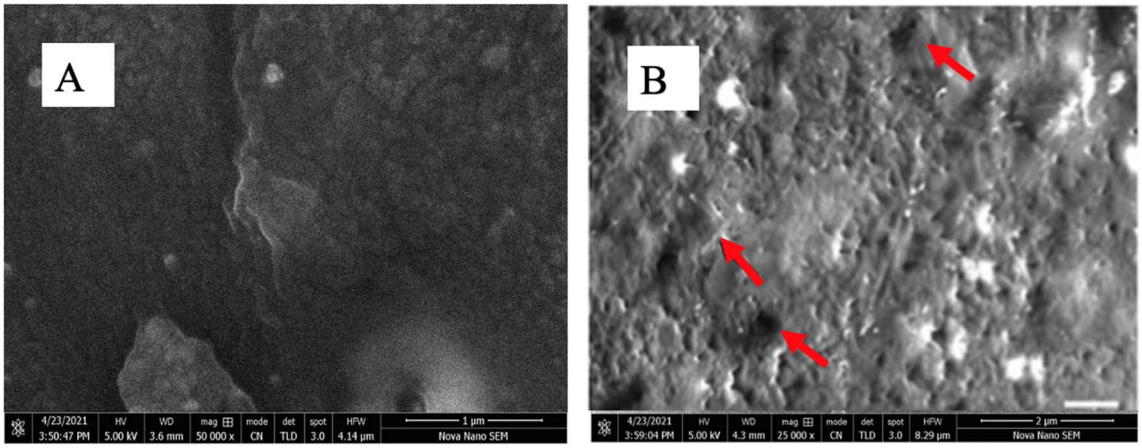

Fig. 8 A = Blank PPY membrane at 500 00× magnification, B = surface morphological analysis of PPY/rGO at 250 00× magnification.

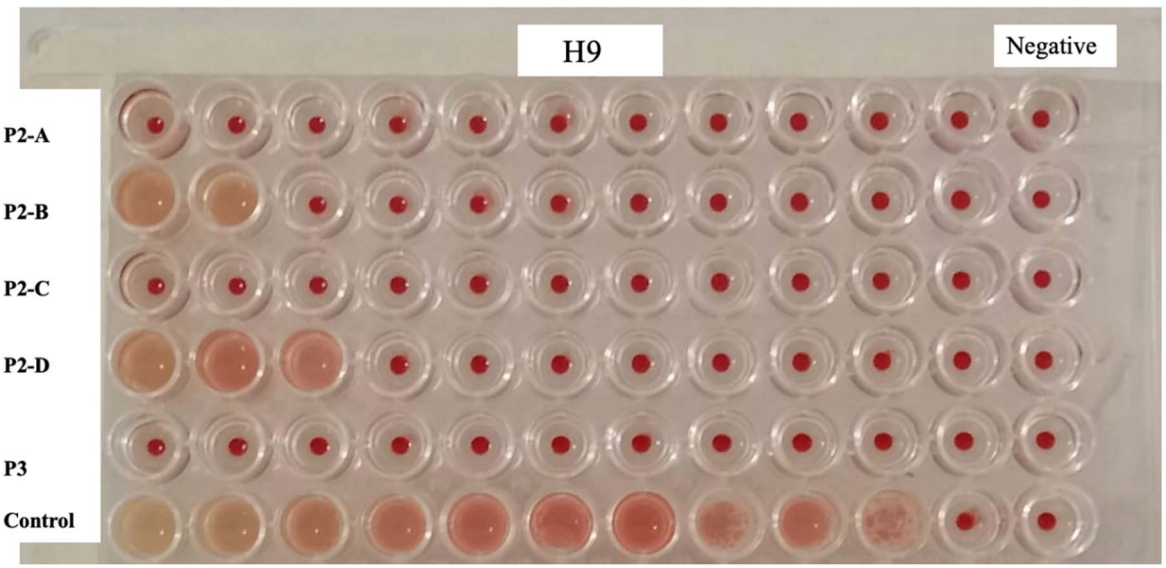

Fig. 9 H9N2 antiviral activity of PPY/metallic-oxide Nps and PPY/rGO membranes against H9N2; where PPYY-A, PPYY-B, PPYY-C, PPYY-D and P3 are PPY/ZnO Nps, PPY/Fe_2O_3 Nps, PPY/CO_3O_4 Nps, PPY/CuO Nps and PPY/rGO membranes respectively.

Table 1 Titration values of HA against Bacteroidales bacterium H9 and IBV for PPY/metallic-oxide Nps and PPY/rGO membranes

	H9N2		IBV	
Membrane	HA titration[a]	Control	HA titration[a]	Control
PPY/ZnO	0	2048	8	1024
PPY/Fe_2O_3	2	2048	2	1024
PPY/CO_3O_4	2	2048	2	1024
PPY/CuO	0	2048	4	1024
PPY/rGO	4	2048	2	1024

[a] Hemagglutination (HA) titer 0–8: strongly effective drug (no growth or very limited growth of virus); 16–32: effective drug (limited growth of the virus, the drug has controlled viral growth effectively); 64–128: moderately effective drug (the drug is not able to control the growth of virus very efficiently, but it is still able to control growth to some extent); 256–2048: ineffective drug (unable to control the growth of virus).

nanoparticle-impregnated membranes, this blank membrane is quite smooth. Fig. 7B and C show the membranes of PPYy/ZnO Nps and PPYy/Fe_2O_3 Nps, respectively. The membrane's surface was visibly rough, representing the existence of NPs. The porous structure of the membranes is represented by the small cracks highlighted by red arrows.

4.4. PPY/rGO membrane characterization

SEM was used to examine the surface morphology of the PPY/rGO membrane. Fig. 8 depicts SEM images of blank PPY and PPY/rGO membranes. These membranes were photographed at a magnification of 25 000 at an accelerating voltage of 5.0 kV for electrons with HFWs of 41.4 μm and 8.29 μm at various magnifications. Fig. 8A shows the smooth surface of the polymer over the aramid fabric; this blank membrane is smoother than the membranes impregnated with rGO. The PPY/rGO membrane is depicted in Fig. 8B. The rough surface of this membrane indicated the presence of impregnated nanomaterial. The porous structure of the membranes is depicted by the small crevices highlighted by red arrows.

4.5. Disinfection ability of PPY/metallic-oxide Nps membranes and PPY/rGO membrane evaluation

All the prepared membranes were examined for antiviral activity against H9N2 (Fig. 9) and IBV (Fig. 10). Table 1 summarizes the performance of PPY/metallic-oxide Nps membranes. According to the data, the membranes demonstrated very little effectiveness against the microorganisms. Among the PPY/metallic-oxide Nps membranes tested, PPY/ZnO Nps and PPY/CuO Nps membranes demonstrated the highest activity against Bacteroidales bacterium, whereas against H9, PPY/Fe_2O_3 Nps, PPY/CO_3O_4 Nps and PPY/rGO exhibited maximum activity against IBV.

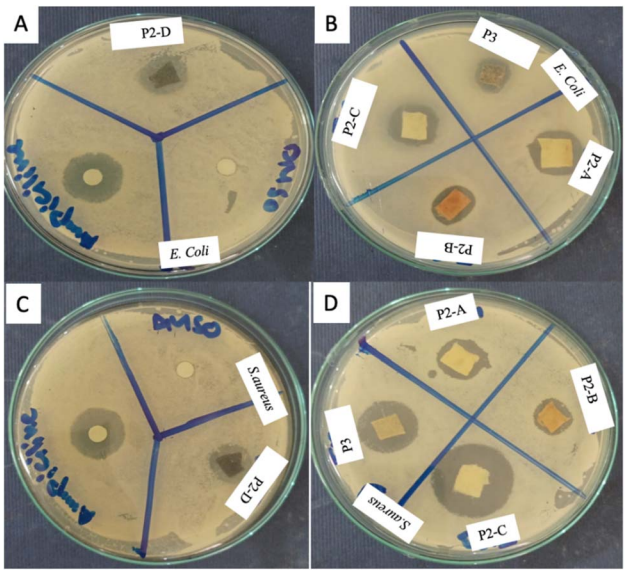

Fig. 11 Zones of inhibition of PPY/metallic-oxide Nps and PPY/rGO membranes against *E. coli* (A and B) and *S. aureus* were determined (C and D). PPYY-A, PPYY-B, PPYY-C, PPYY-D, and P3 represent PPY/ZnO Nps, PPY/Fe_2O_3 Nps, PPY/CO_3O_4 Nps, PPY/CuO Nps, and PPY/rGO membranes, respectively.

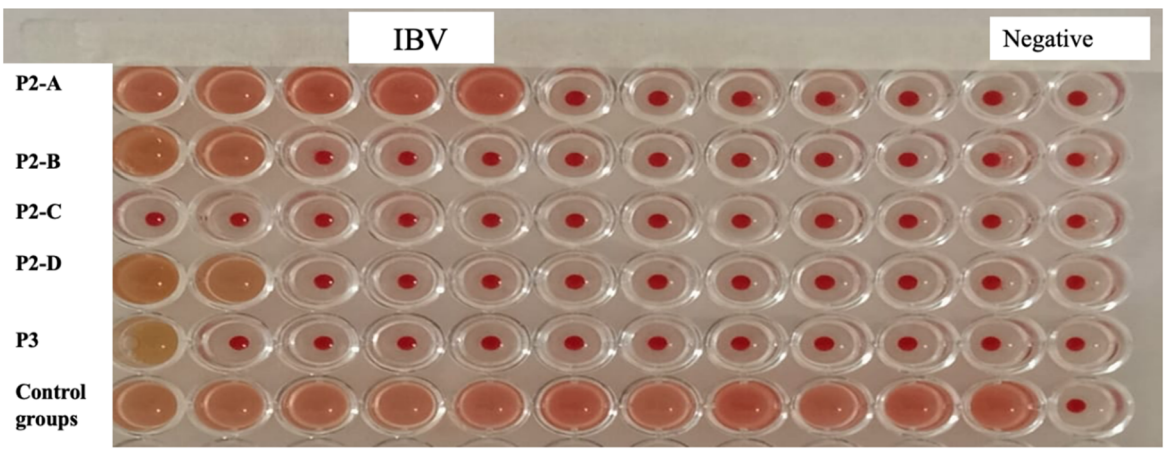

Fig. 10 IBV antiviral activity of PPY/metallic-oxide Nps membranes; where PPYY-A, PPYY-B, PPYY-C, PPYY-D and P3 are PPY/ZnO Nps, PPY/Fe_2O_3 Nps, PPY/CO_3O_4 Nps, PPY/CuO Nps and PPY/rGO membranes respectively.

Table 2 Zone of inhibition values of PPY/metallic-oxide Nps and PPY/rGO membranes against *E. coli* and *S. aureus*

	E. coli		*S. aureus*	
Membrane	Zone of inhibition	Control	Zone of inhibition	Control
PPY/ZnO	07	22	05	22
PPY/Fe_2O_3	12	22	07	22
PPY/CO_3O_4	08	22	02	22
PPY/CuO	02	22	08	22
PPY/rGO	08	22	09	22
DMSO	07		07	

All the membranes prepared were assessed for their antibacterial activity against *E. coli* and *S. aureus* (Fig. 11). DMSO and Ampicillin were employed as positive and negative controls in the experiments, respectively. Table 2 summarizes the performance of PPY/metallic-oxide Nps membranes. According to the results, the PPY/Fe_2O_3 Nps membrane had the highest activity against *E. coli*, where PPY/rGO produced the best results against *S. aureus*.

5. Conclusion

Our study presents a novel approach to enhancing polypropylene hybrid polymeric membranes for water purification applications by incorporating metallic nanoparticles and reduced graphene oxide (rGO). The characterization of these membranes using FTIR spectrometry, SEM, and UV-Vis Spectrophotometry confirmed their improved antimicrobial and antiviral properties, as evidenced by the effective disinfection capabilities against bacterial strains *S. aureus* and *E. coli*, as well as H9N2 and IBV strains of viruses. These results align with previous research demonstrating the antimicrobial and antiviral efficacy of nanomaterial-enhanced membranes.[32,33] Our study further highlights the synergistic effects of combining multiple nanomaterials, contributing to the development of more efficient water purification technologies.

In conclusion, the incorporation of metallic nanoparticles and rGO into polypropylene hybrid polymeric membranes is promising to improve water purification processes, addressing pressing challenges in public health and environmental sustainability. The findings of this study underscore the potential of nanomaterial-enhanced membranes as effective tools for combating waterborne pathogens and advancing the field of membrane-based water treatment. As a take-home message, our research emphasizes the importance of interdisciplinary approaches in developing innovative global water quality management solutions.

6. Future insights

In the evolving landscape of water purification technology, the quest for durable and efficient membranes continues. Incorporating reduced graphene oxide (rGO) and metallic nanocomposites into polypropylene membranes has already shown promise in enhancing antimicrobial properties and combatting biofouling. Future research is likely to delve into augmenting the durability and broadening the antimicrobial spectrum of these membranes to counteract a wider array of pathogens, including resilient multi-drug resistant strains. Alongside this, the pursuit of environmentally benign materials is essential to ensure that the end-of-life disposal of these membranes does not contribute to ecological damage. The synergy between rGO and various metallic nanoparticles presents an intriguing avenue for boosting membrane functionality, potentially leading to superior pollutant selectivity and flow efficiency performance. Cost-effective production methods are also pivotal in making these innovative membranes viable for widespread application, particularly in large-scale water treatment facilities. Testing under real-world conditions will remain crucial, necessitating the compatibility of advanced membranes with existing infrastructure to ensure seamless integration. Additionally, developing simple yet effective membrane regeneration and cleaning protocols will contribute to sustainability by extending the membranes' functional life. Ultimately, the impact of these advanced membranes on public health, especially in regions grappling with water quality issues, will be a significant measure of their success, potentially heralding a new era in the field of membrane-based water treatment.

Conflicts of interest

The authors declare no conflict of interest.

Acknowledgements

The authors acknowledge Higher Education Commission of Pakistan's NRPU program (project #10312) for supporting the project.

References

1 E. O. Ezugbe and S. Rathilal, *Membranes*, 2020, **10**, 89.
2 L. Pang, J. Meier-Haack, S. Huang, L. Qi, H. Cui, S. Ruan, *et al.*, *Adv. Sustainable Syst.*, 2021, **5**, 2000279.
3 Y. Oshiba, Y. Harada and T. Yamaguchi, *J. Membr. Sci.*, 2021, **619**, 118772.
4 Y.-H. Wang, Y.-H. Wu, X. Tong, T. Yu, L. Peng, Y. Bai, *et al.*, *Water Res.*, 2019, **154**, 246–257.
5 D. Suresh, P. S. Goh, A. F. Ismail and N. Hilal, *Membranes*, 2021, **11**, 832.
6 P. M. Jadhav, S. Kantevari, A. B. Tekale, S. V. Bhosale, R. P. Pawar and S. U. Tekale, *Phosphorus, Sulfur Silicon Relat. Elem.*, 2021, **196**, 879–895.
7 M. Ayub, S. Z. H. Naqvi, W. Ahmad, M. M. Arif, K. A. Saqib, A. Hameed, *et al.*, *J. Pak. Inst. Chem. Eng.*, 2022, **50**, 57–70.
8 R. Desiriani, H. Susanto, T. Istirokhatun, Y. Lin, N. Aryanti, H. Abriyanto, *et al.*, *J. Environ. Chem. Eng.*, 2024, **12**, 111797.
9 Z. Sargolzaei, F. Nabizadeh Chianeh, M. Shamsodin and J. Porous, *Mater*, 2023, **30**, 377–386.
10 K. Mustafa, N. Iqbal, S. Ahmad, I. Hussain and S. Musaddiq, *Korean J. Chem. Eng.*, 2023, **40**, 2735–2743.

11 J. Sackey, A. Fell, J. B. Ngilirabanga, L. C. Razanamahandry, S. K. O. Ntwampe and M. Nkosi, *Mater. Today: Proc.*, 2021, **36**, 336–342.
12 S. Ramos, V. Silva, M. D. L. E. Dapkevicius, M. Caniça, M. T. Tejedor-Junco, G. Igrejas, *et al.*, *Animals*, 2020, **10**, 2239.
13 S. Singh, A. Numan, H. H. Somaily, B. Gorain, S. Ranjan, K. Rilla, *et al.*, *Mater. Sci. Eng. C*, 2021, **129**, 112384.
14 M. Li, G. Huang, X. Chen, H. Xiao, C. An, J. Yin, *et al.*, *Chem. Eng. J.*, 2024, **481**, 148744.
15 B. E. Rodríguez, M. M. Armendariz-Ontiveros, R. Quezada, E. A. Huitrón-Segovia, H. Estay, A. García García, *et al.*, *Polymers*, 2020, **12**, 2860.
16 A. K. Shukla, J. Alam, M. A. Ansari, M. Alhoshan and F. A. A. Ali, *Environ. Sci. Pollut. Res.*, 2018, **25**, 34103–34113.
17 S. D. Chavan, S. R. Mirgane and R. D. More, *J. Eng. Sci.*, 2020, **11**, 1413–1416.
18 M. S. H. Bhuiyan, M. Y. Miah, S. C. Paul, T. D. Aka, O. Saha, M. M. Rahaman, *et al.*, *Heliyon*, 2020, **6**, e04603.
19 Y. Yulizar, D. O. B. Apriandanu and Y. Pratiwi, *Mater. Sci. Forum*, 2020, **982**, 9–13.
20 D. R. A. Preethi and A. Philominal, *Mater. Lett.: X*, 2022, **13**, 100122.
21 H. Javaid, K. Mustafa, M. Khan, S. Iqbal, S. Ahmad, M. Rani, *et al.*, *Chem. Phys.*, 2023, **573**, 112019.
22 K. Sharma, M. Kumar, R. Waghmare, R. Suhag, O. P. Gupta, J. M. Lorenzo, *et al.*, *Int. J. Biol. Macromol.*, 2022, **209**, 763–778.
23 M. Meerwein, A. Tarnutzer, M. Böni, F. Van Bambeke, M. Hombach and A. S. Zinkernagel, *Antibiotics*, 2020, **9**, 218.
24 M. Rajbhandari, U. Wegner, M. Jülich, T. Schoepke and R. Mentel, *J. Ethnopharmacol.*, 2001, **74**, 251–255.
25 H. Rehman, Z. Ali, M. Hussain, S. Gilani, T. Shahzady, A. Zahra, *et al.*, *Digest J. Nanomater. Biostruct.*, 2019, **14**, 1033–1040.
26 M. Hafeeza, R. Shaheena, S. Alib, H. A. Shakirc, M. Irfand, T. A. Mughalb, *et al.*, *Digest J. Nanomater. Biostruct.*, 2021, **16**, 899–906.
27 P. Ahamed and M. A. Yousuf, *Adv. Mater. Phys. Chem.*, 2020, **10**, 111–124.
28 M. Elango, M. Deepa, R. Subramanian and A. Mohamed Musthafa, *Polym.-Plast. Technol. Eng.*, 2018, **57**, 1440–1451.
29 D. Balram, K.-Y. Lian and N. Sebastian, *Ultrason. Sonochem.*, 2019, **58**, 104650.
30 P. B. Koli, K. H. Kapadnis, U. G. Deshpande and M. R. Patil, *J. Nanostruct. Chem.*, 2018, **8**, 453–463.
31 R. Rajamma, S. Gopalakrishnan Nair, F. Abdul Khadar and B. Baskaran, *IET Nanobiotechnol.*, 2020, **14**, 833–838.
32 A. C. Mecha, M. N. Chollom, B. F. Babatunde, E. K. Tetteh and S. Rathilal, *Membranes*, 2023, **13**, 432.
33 Er S. Gungordu, M. Edirisinghe and T. A. Tabish, *Adv. Healthcare Mater.*, 2023, **12**, 2201523.